NUCL SCI TECH (2020) 31:28
https://doi.org/10.1007/s41365-020-0737-5

Spin coating of TPB film on acrylic substrate and measurement of its wavelength shifting efficiency

Hang Yang[1] · Zi-Feng Xu[1] · Jian Tang[1] · Yi Zhang[2]

Received: 3 September 2019 / Revised: 15 December 2019 / Accepted: 14 January 2020 / Published online: 25 February 2020

Abstract Scintillation light from a liquid noble gas during a neutrino or dark matter experiment lies typically within the vacuum ultraviolet region and might be strongly absorbed by surrounding materials such as light guides or photomultipliers. Tetraphenyl butadiene (TPB) is a fluorescent material, acts as a wavelength shifter, and can turn UV light into visible light at a peak wavelength of approximately 425 nm, enabling the light signals to be easily detected during physics studies. Compared with a traditional TPB coating method using vapor deposition, we propose an alternative technique applying a spin-coating procedure to facilitate the development of neutrino and dark matter detectors. This article introduces a method to fabricate a TPB film on an acrylic substrate by using a spin-coating method, reports the measurements of the sample film thickness and roughness, demonstrates the reemission spectrum, and quantifies the wavelength shifting efficiency.

Keywords Wavelength shifter · Tetraphenyl butadiene · Spin-coating method

This study was supported in part by the Guangdong Basic and Applied Basic Research Foundation (No. 2019A1515012216), the National Natural Science Foundation of China (No. 11505301) and the Innovation Training Program for bachelor students at the School of Physics in SYSU.

Hang Yang and Zi-Feng Xu have contributed equally to this work.

✉ Jian Tang
tangjian5@mail.sysu.edu.cn

[1] School of Physics, Sun Yat-sen University, Guangzhou 510275, China

[2] School of Chemistry, Sun Yat-sen University, Guangzhou 510275, China

1 Introduction

A wavelength shifter (WLS) is critical to modern liquid noble gas detectors. It converts an ultraviolet light signal into a visible light signal of a particular wavelength. The wavelength of scintillation light from liquid noble gas is in the vacuum ultraviolet (VUV) range, varying from 80 to 200 nm. The light within this wavelength range is strongly absorbed by most detector materials. Tetraphenyl butadiene (TPB) is one of the popular WLS options [1–3] used in a number of neutrino and dark matter experiments applying liquid argon, such as MicroBooNE [4], DUNE [5], DEAP-3600 [6, 7], DarkSide-20k [8], and ArDM [9], which absorbs UV light and reemits light within the visible spectrum to be easily and effectively detected by photomultiplier tubes (PMTs) or silicon photomultipliers (SiPM). WLS is also used in Cherenkov detectors to improve the light yield [10–12]. It is important during current and next-generation experiments to find a cost-effective way to coat the TPB on the surface of the detector container.

A vapor deposition method [13] is commonly used in TPB film fabrication, and in [14], a spraying method is proposed. Because the vapor deposition method requires a high vacuum and a spraying method allows no control of the film thickness, we propose the fabrication of a TPB film using the spin-coating method, which can act as an alternative option. The primary purpose of this study is to make TPB films using a spin-coating method and measure the film geometry and its capability of shifting the UV light. The light shifting capability of a TPB material is called the quantum efficiency (QE), which is defined as the average number of photons that TPB reemits when it absorbs a single photon. The QE is an intrinsic property of the

material itself and is independent of the film condition, e.g., the thickness and roughness. Because it is difficult to obtain a single photon as incident light, it is difficult to measure the QE directly. Therefore, the shifting capability of an entire film under multiphoton incident light, which is called the wavelength shifting efficiency (WLSE), is measured instead. The WLSE is a result of the folding QE based on the condition of the film and the optical configuration, and is a more straightforward representation of the TPB film performance in physics applications.

Although UV light from most liquid noble gases has a wavelength of below 200 nm and cannot transport much longer distances in air or in an acrylic form, in [1] a clear relationship between the WLSE and incident light at different wavelengths is shown. The WLSEs at different wavelengths share similar trends when they vary with the film thickness [15]. This enables us to conduct our WLSE measurement at a selected wavelength of 254.5 nm, even without a vacuum environment. TPB is known to form at least four polymorphic types of crystals, depending on the deposition method applied [16, 17]. The optical response at 250 nm includes the absorption, and consequently, the WLSE of these different types of TPB can be quite different [18]. It is also known that the scintillation yield of macroscopic TPB crystals grown from a solution is much higher than the yield of the evaporated coatings [19, 20]. Despite the differences in the deposition method, it is assumed that the main results will still hold up in the same way.

In this study, we first propose a different TPB coating technique in Sect. 2. In Sect. 3, we then describe the experimental setup used to measure the optical properties from our TPB samples. in Sect. 4, an analysis method follows to quantify the WLSE with an emphasis on the geometrical acceptance ratio corrections. In Sect. 5, we report the light reemission spectrum by our TPB samples and make a comparison of the WLSE between our results and those reported in a recent study. Finally, we provide a summary of this research and some concluding remarks.

2 Fabrication with spin coatings

Without a loss of generality, we choose an acrylic disk as the base material for a demonstration of the TPB coatings owing to its high transparency within the wavelength region of interest. A description of the spin-coating procedure is shown in Fig. 1.

Methylbenzene was used as the solvent for the TPB powder, and its capability has been previously described [21]. According to [22], the spinning speed is the major factor affecting the thickness of the film, whereas the duration does not have much significance.

We first sanded the surface of the acrylics and applied a TPB solution to the target surface with methylbenzene as our solvent. According to a previous study [23, 24], the TPB solution is then spread during stage 1 and the solvent methylbenzene volatilizes during stage 2. In this way, stage 1 has the greatest effect on the thickness of the film as the TPB is carried in the spreading solution. We conducted preparative experiments to find the proper speed and the duration for stage 1. A small amount of solution is spread during stage 2 owing to its viscosity, and the sample thickness will no longer change, which allows us to choose the parameters for stage 2 based on experience without a loss of generality.

The solubility of TPB in methylbenzene was roughly 0.021 g/ml based on weight measurements conducted at room temperature. A concentration of 0.02 g/ml was chosen for the fabrication of the samples. The acrylic substrate in a round shape was fixed on the spinning platform of the spin-coating machine by a vacuum pump. The TPB solution was manually added to the center of the acrylic disk. The spinning process consists of two stages with different speeds and durations. Various combinations of speed and duration were used in a preparative experiment. The key parameters used to prepare the samples during the spin-coating procedure are summarized in Table 1.

After the spinning procedure, the sample was placed on a heated table at 70 °C for 2 min for drying. As determined experimentally, the temperature and duration might not be significant if the film is completely dried.

The fabricated sample appears to be rather uniform and stable when touched by the finger. Further surface measurements using SEM were conducted and are given in Fig. 2.[1] We saw tiny holes, which might have been caused by the fast heating and drying processes. The more uniformly the TPB film is fabricated, the better the fabrication method is applied during the particle experiments. An investigation into the application of a proper temperature and curing process to improve the surface roughness is warranted. Samples were preserved in a dark environment to prevent degradation [25, 26].

We then measured the thickness and roughness of different TPB films made using a spin-coating method. A profilometer was applied for this purpose. Each sample was scratched using a piece of metal to create a notch as a requirement of the profilometer.

The left panel in Fig. 3 is a photograph of an acrylic disk coated with a TPB film. Special types of samples, which have only half of the surface covered by a TPB film, shown in the right-side panel of Fig. 3, were made for roughness and thickness measurements. These special samples were

[1] The measurement was conducted on November 1, 2019. The raw SEM image shows the wrong date owing to a software issue.

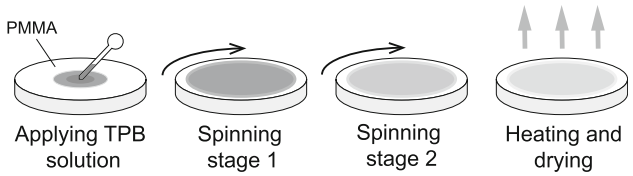

Fig. 1 Spin-coating procedure

Table 1 Parameters

Stage 1	Speed	700 r/min
	Duration	6 s
Stage 2	Speed	1000 r/min
	Duration	20 s
Concentration		0.02 g/ml

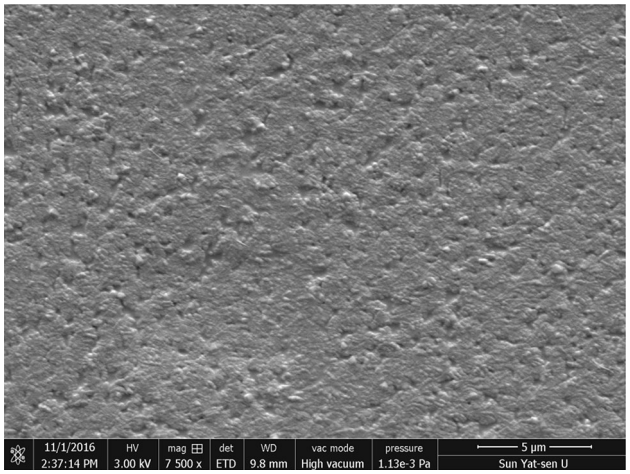

Fig. 2 The surface profile measured using a scanning electron microscope (SEM) at the 5-µm scale

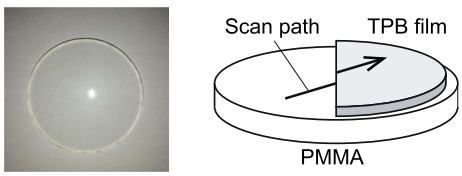

Fig. 3 A photograph of the fabricated sample is shown in the left panel. Half-coated samples of TPB and the scanning path based on the profilometer are shown in the right panel

created using the same parameters used during the fabrication process except half of their surfaces were protected by a blank paper film before the TPB solution was added. The paper film was removed after the TPB solvent was completely dried. It was assumed that this half-pearl paper film would not affect the thickness and roughness of the TPB film. Figure 4 shows the scanning results of a half-coated TPB film and a film scratched using a profilometer. Each scan covered a 4-mm-long path and provided the height along the path. It is thus safe to consider the results of these paths as representing the properties of the entire film because the film is almost uniformly distributed [27]. The peak at the boundary in the half-coated TPB sample was caused by a protection film used during the fabrication process. We consider this accumulation as the result of a wet edge between the solution and the final film and assume that the edge does not affect the TPB-coated area far from the boundary. Thus, this peak is ignored during the following steps.

In the result of a half-coated sample, the profilometer scan path covered an edge of the TPB film such that both surfaces of the TPB film and the acrylic substrate were included. The average height of the coated part with respect to the substrate was considered as the thickness, and the uncertainties in the measurement of the unscratched part was considered as a representation of the roughness. The measurements were repeated several times, the results of which are shown in Table 2. The scans for the scratched samples also used a 4-mm path. The obvious valley indicates the scratch applied purposefully. The difference between the bottom of the valley and the baseline is considered the thickness of this sample.

As shown in Table 2, the thickness of TPB fabricated using the spin-coating method was thinner than the reported result made through the vapor deposition. Therefore, it was expected that the WLSE herein was slightly lower than the thicker sample produced by the vapor deposition.

3 Experimental setup

All apparatuses used in experiment are listed in Table 3. A custom apparatus setup was built for measurements of the spectrum and photocurrent. A schematic of this setup is shown in Fig. 5.

We take a mercury lamp with a filter installed right in front of the light exit window as the light source. The lamp provides light waves ranging from 245 nm to 405 nm according to the characteristic spectrum of mercury. The spectra of the source light and reemission light overlap at a wavelength of approximately 400 to 420 nm, which hinders our optical measurement. Therefore, a second filter, an interference filter with a transmission peak at a wavelength of 254.5 nm, was introduced to generate an incident monochromatic light.

Herein, the upper surface of the filter or TPB film is considered as a light source. The spectrum measurements of both incident light and reemission light are conducted using a fiber spectrometer. The entrance of the fiber was placed at a fixed position and angle. The counting of the

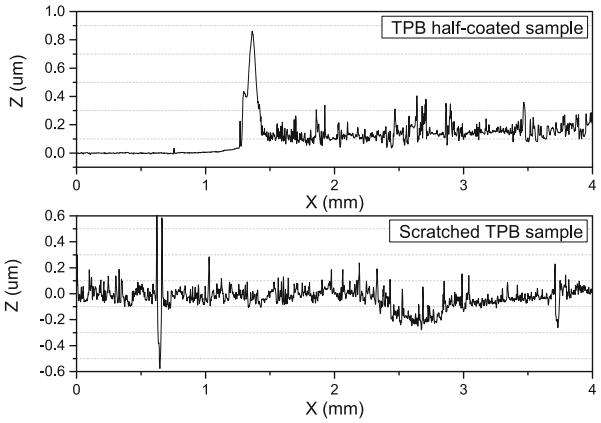

Fig. 4 Results of the half-coated TPB and scratched samples using profilometer scans

Table 2 Profilometer results

Measurements	Thickness (μm)	Roughness (μm)
1	0.15	0.051
2	0.17	0.100
3	0.22	0.074
4	0.19	0.081
Average	0.18	0.076

The roughness is represented by the standard error of the thickness data

Table 3 A list of apparatuses for optical measurements

Apparatus	Type
Spectrometer	Ocean 2000 [28]
Profilometer	KOSAKA ET150 [29]
UV light	WFH-204b [30]
The filter	Shengyakang
Si Photodiode	LXD-66MQ
Spinner	KW-4A [31]
Voltmeter	DM3000 Series [32]

photocurrent was achieved using a silicon photodiode. Owing to the strong absorption of UV light in air, the light sensor, i.e., the photodiode or fiber entrance, was placed as close to the light source as possible, meaning that the detector touches either the lower surface of the filter or the acrylic substrate.

A DC power of 5 V was supplied to the silicon photodiode set to work in photoconductive mode, which was not compulsory but can slightly improve the photocurrent measurements. The photodiode had been calibrated by the vendor. This spectrometer covered the range from 200 to 800 nm. After a careful calibration, the fiber was supposed to avoid bringing about systematic uncertainties. As the data were supplied during each measurement, ambient noise in the laboratory environment was measured and subtracted with the help of a control and analysis software. In principle, the two configurations used in the optical measurement had slightly different geometries. A geometry-related correction is considered in our later analysis.

4 Analysis methods

WLSE is defined as the ratio between the reemission light intensity and the incident light intensity produced by the coated film. We first establish an optical model to help with the data analysis. For a monochromatic light at a wavelength of λ, each photon with an energy of $\frac{hc}{\lambda}$ caused a photocurrent of $\frac{hcR}{\lambda}$, where R is the response of the photodiode [33]. Hence, the number of photons n can be calculated using the photocurrent in the following equation:

$$n \propto \frac{I}{\frac{hcR}{\lambda}}. \tag{1}$$

Given a continuous light spectrum of $S(\lambda)$ (a normalized factor), this equation can be transformed into the following:

$$n \propto \frac{I}{\int \mathrm{d}\lambda \frac{hc}{\lambda} R(\lambda) S(\lambda)}. \tag{2}$$

Hence, the WLSE would be as follows:

$$\mathrm{WLSE} = \frac{I_{\mathrm{TPB}}}{I_{\mathrm{incident}}} \times \frac{\int \mathrm{d}\lambda' \frac{hc}{\lambda'} S_{\mathrm{incident}}(\lambda') R(\lambda)}{\int \mathrm{d}\lambda'' \frac{hc}{\lambda''} S_{\mathrm{TPB}}(\lambda'') R(\lambda)} \times \frac{1}{A}, \tag{3}$$

where A is a geometrical acceptance ratio which roughly represents the geometrical difference of the apparatus configurations used to measure I_{incident} and I_{TPB}. The numerical value for the ratio of two integrals in the middle of Eq. (3) is 0.96. In general, we need to measure the photocurrent I_{incident}, I_{TPB} using a photodiode, and spectrum S_{TPB}, S_{incident} using a fiber spectrometer. To measure the photocurrent of the light source, first, the TPB film was removed and the filter surface was considered as our light source. Next, during a measurement of the reemission photocurrent, the TPB film was considered as the light source. The photodiode was placed as close to the light source as possible during each measurement. Thus, the distance between the photodiode and light source is determined by the thickness of the acrylics or filter. Because the filter was thinner, the Si photodiode received more light in the light source measurement because it was indeed closer to the light source. A geometrical acceptance ratio was introduced to consider the difference and make

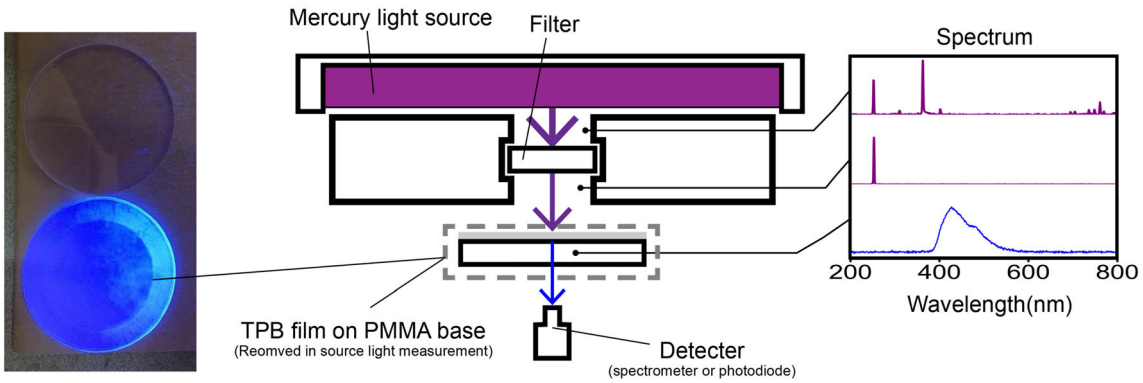

Fig. 5 (Color online) Experiment setup used to measure the reemission spectrum using a spectrometer or the photocurrents using a photodiode

our measurements more accurate and self-consistent. This factor was determined by the geometry of the apparatus configurations, which was simplified into the model shown in Fig. 6 by means of geometrical optics.

Among the dimensions marked in Fig. 6, r_2 and D were measured in the laboratory with a precision of 0.01 mm, whereas L was provided by the vendor. These values were considered during the error propagations. Although the uncertainty in L was not provided, we took a conservative uncertainty at 0.2 mm. The other parameters such as r_1 and h were also measured using a micrometer but ignored in the error propagation because their influence was determined to be less than 0.1% in our estimation. To summarize, uncertainties of r_2, D, and L were considered and processed for a further quantitative analysis.

Both the source light and reemission light are considered as an even circular area Lambert source of the same size. The silicon photodiode has a sensitive square-shaped area. Suppose that P (x_1, y_1) is a point on the area light source and Q (x_2, y_2) is a point on the photodiode. The intensity of light, as measured by a luminous flux, received by Q will

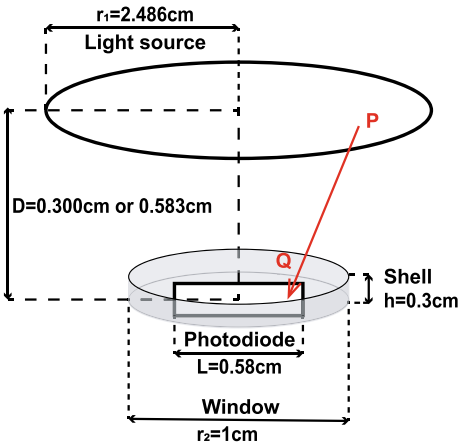

Fig. 6 Simplified model for geometrical acceptance ratio calculation. $D = 0.583$ cm for the reemission measurement and $D = 0.300$ cm for the source light measurement

decrease if Q is far from P or deviate from the exact front of P, and for a Lambert light source, Q will receive the following luminous flux:

$$\mathrm{d}I_{\mathrm{Q}} = B\frac{\cos^2\theta}{r^2}\mathrm{d}S_{\mathrm{P}}\mathrm{d}S_{\mathrm{Q}}, \tag{4}$$

where $\mathrm{d}S_{\mathrm{P}}$ and $\mathrm{d}S_{\mathrm{Q}}$ are surface elements near P and Q, respectively, and B represents the brightness. Because we are interested in their ratio, it is safe to take the brightness B as 1.

In terms of the light reemission, there are two major factors that can reduce the intensity of light. First, a reflection occurs when light enters the surface of the acrylic disk. Herein, we ignore multiple reflections such that the reflected light will simply be lost. Second, light will be attenuated exponentially in the acrylics. However, an acrylic substrate is extremely thin, whereas the light attenuation length in the acrylics at 420 nm is more than 1 m according to previous measurements [34]. This means that the attenuation effect will be extremely weak. A simple estimate tells us that the difference caused by an exponential attenuation should be less than 0.5%. Therefore, the attenuation effect can be safely ignored here. In conclusion, an extra reflection factor has to be included to describe a reduction in the light intensity owing to the reflections occurring on the acrylics. The transmission factor T remains the same when swapping indexes 1 and 2 in Eq. (6). Thus, T is simply factored in twice.

$$\mathrm{d}I_{\mathrm{Q}} = B\frac{\cos^2\theta}{r^2}T^2\mathrm{d}S_{\mathrm{P}}\mathrm{d}S_{\mathrm{Q}}, \tag{5}$$

where

$$T(\theta) = 1 - \left(\frac{1}{2}r_p^2 + \frac{1}{2}r_s^2\right) = 1 - \frac{1}{2}\left[\frac{\tan(\theta_1-\theta_2)}{\tan(\theta_1+\theta_2)}\right]^2 - \frac{1}{2}\left[\frac{\sin(\theta_1-\theta_2)}{\sin(\theta_1+\theta_2)}\right]^2, \quad n_1\sin\theta_1 = n_2\sin\theta_2. \tag{6}$$

The transmission factor T is calculated according to the Fresnel formula, assuming that incident light is not polarized there with equal contributions from the P-wave (parallel) and S-wave (transverse). The calculation requires two refractive indices from the air and acrylics, namely $n_1 = 1$ and $n_2 = 1.489$, based on the work in [35]. Figure 7 shows how the reflection factor varies with the angle of incident light.

It is necessary to integrate over the surface as follows to obtain the ratio of light intensity at the source and the light intensity received by a photodiode:

$$G = \frac{I_{\mathrm{Q}}}{I_{\mathrm{all}}} = \frac{1}{I_{\mathrm{all}}} \iiiint_{\text{boundary}} \mathrm{d}I_{\mathrm{Q}}. \tag{7}$$

Note that the transmission factor only appears in the reemission light measurement. Here, I_{all} is the total intensity at the light source, which has the same value in both setups and thus cancels each other out in the ratio. The boundary of (x_1, y_1) and (x_2, y_2) is a circle and square, respectively, with dimensions shown in Fig. 6. Parameter D is 0.300 cm for the source light measurement and 0.583 cm for the reemission measurement. Note that the shell of the photodiode can potentially block the light. This is cross-checked and safely treated in the integral, which is then calculated numerically. The parameter G represents the light detection efficiency of a photodiode. The geometrical acceptance ratio A for different setups is given by the following:

$$A = \frac{G_{\mathrm{reemission}}}{G_{\mathrm{source}}}. \tag{8}$$

We immediately calculate the results for $G_{\mathrm{reemission}} = 59.28$ and $G_{\mathrm{source}} = 69.86$. We then obtain the geometrical acceptance ratio at 0.848. This value is smaller than 1, indicating that the photodiode is less likely to receive the reemission light than the source light, which is mainly because the acrylic surface reflects the former. Because the light source is much larger than the photodiode, this factor is insensitive to a horizontal movement of the photodiode, which provides a high tolerance for the deviation of photodiode placement by hand. As mentioned above, the geometrical acceptance ratio A is determined by r_2, D, and L. Errors among the measured values will eventually be propagated in the results.

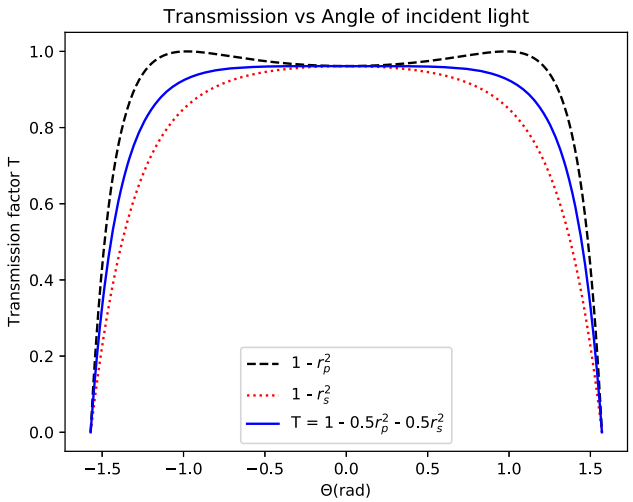

Fig. 7 (Color online) The transmission factor T varies with the angle of incident light

5 Results

5.1 Photocurrent and spectra

The spectra of incident light and reemission light are shown in Fig. 8. The reemission spectrum matches the results reported in Ref. [1], which indicates that the solvent and coating process will not affect the TPB properties.

These spectra will be used in the calculation of the WLSE.

A 100 kΩ resistor is connected to the photodiode in series for reading out the voltage of the photocurrent. Note that this resistor value will be canceled at a particular ratio and in the end will not contribute to any uncertainties. We actually replace the photocurrent with the generated

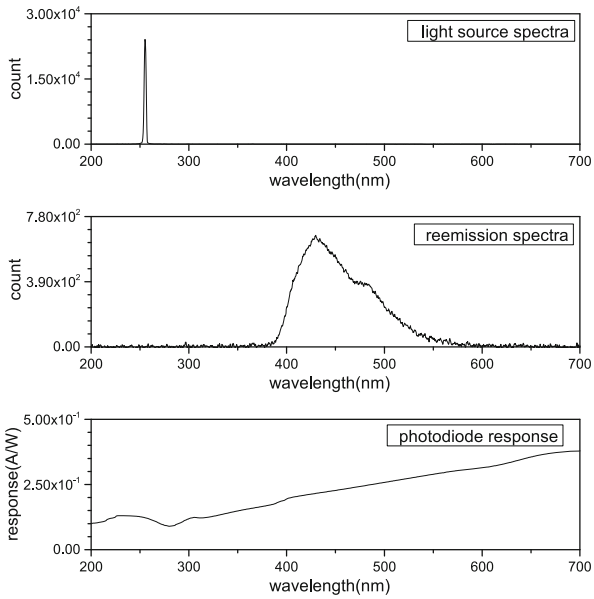

Fig. 8 UV light source, TPB reemission spectrum, the response spectra of the Silicon photodiode

Table 4 A list of uncertainties in the measurements

Index (i)	Name	SD (S_i)	Precision (u_i)	($\partial f/\partial x_i$)	Measuring times
1	U_i	8.394	0.0001 mV	− 0.00074	23
2	$U_{i-\mathrm{dark}}$	0.075	0.0001 mV	0.00074	5
3	U_r	1.881	0.0001 mV	0.0033	24
4	$U_{r-\mathrm{dark}}$	0.108	0.0001 mV	− 0.0033	6
5	r_2		0.01 mm	0.042	1
6	D		0.2 mm	− 0.049	1
7	L		0.2 mm	− 0.0054	1

voltage signal in Eq. (3) to avoid measuring the resistor, which brings about an extra uncertainty.

To guarantee the validity of our results, photocurrent measurements of the light source and the TPB reemission were carried out 6 and 11 times, respectively. The UV light source was turned off between each measurement to avoid an increase in the photodiode temperature, which will further affect the photocurrent. The photocurrent is 341.8 ± 8.4 mV, which is labeled as U_{i} in the source light measurement, and 79.6 ± 1.9 mV in the reemission measurement, which is labeled as U_{r}, with the error being the standard deviation. The dark current is 4.1 ± 0.1 mV, which is labeled as $U_{\mathrm{i-dark}}$ in the source light measurement, and 4.8 ± 0.1 mV in the reemission measurement, which is labeled as $U_{\mathrm{r-dark}}$. The dark current is then subtracted during the analysis.

5.2 Uncertainties

As mentioned above, we must consider the uncertainty of the WLSE propagated from the voltage signals and the geometric measurements. For the voltage measurements, we have to include the incident light voltage, reemission light voltage, and their respective dark counts. The precision of the voltmeter used goes to a level of 0.0001 mV. The statistical uncertainty comes from the standard deviation of the light voltage with its own dark voltage subtracted. The systematic error is calculated according to the precision of our voltmeter. The partial derivatives WLSE with respect to these values will then be calculated analytically. For geometric measurements, we also use the standard deviations as statistical errors and calculated the systematic errors from the precision using a micrometer. Note that these values take part in the numerical integral in Eq. (7). Thus, the partial derivatives of the WLSE will be calculated numerically.

We present a list of uncertainties in Table 4, which covers all values we measured along with their precision and standard deviation (Stdev). The notation for each value is defined there as well. If we define the combined statistical uncertainty S_{A} with ν_{A} as its degree of freedom and the systematic uncertainty S_{B} with ν_{B} as its degree of freedom, we can list the formula and results of the error propagations as follows:

$$S_{\mathrm{A}} = \sqrt{\sum_{i=1}^{4} (\partial f/\partial x_i \times S_i)^2}, \tag{9}$$

$$\nu_{\mathrm{A}} = \frac{S_{\mathrm{A}}^4}{\sum_{i=1}^{4} \frac{(\partial f/\partial x_i \times S_i)^4}{\nu_i - 1}}, \tag{10}$$

$$S_{\mathrm{B}} = \sqrt{\sum_{i=1}^{7} (\partial f/\partial x_i \times u_i)^2}, \tag{11}$$

$$\nu_{\mathrm{B}} = \frac{S_{\mathrm{B}}^4}{\sum_{i=1}^{7} (\partial f/\partial x_i \times u_i)^4}, \tag{12}$$

$$S = \sqrt{S_{\mathrm{A}}^2 + S_{\mathrm{B}}^2}, \tag{13}$$

$$\nu = \frac{S^4}{\frac{S_{\mathrm{A}}^4}{\nu_{\mathrm{A}}} + \frac{S_{\mathrm{B}}^4}{\nu_{\mathrm{B}}}}. \tag{14}$$

We checked the coverage factor t_p and the corresponding degrees of freedom ν from the t-distribution table [36]. The uncertainty of the WLSE can be obtained as $\Delta\mathrm{WLSE} = t_p S = 0.044$ at the 95% confidence level (C.L.).

5.3 WLSE

The result of the WLSE based on our TPB samples is 0.251 ± 0.044 on average at 95% C.L. This result is in line with the trend of the measurements described in [1], where the WLSE of a 0.7 μm TPB film is approximately 0.4 μm. (The thicknesses of our samples are approximately 0.18 μm, as shown in Table 2.) Recall that the WLSE as a property of the film is determined by the intrinsic property of the TPB material, the QE, and the optical setup. It is therefore reasonable to expect that the WLSE here will decrease as the film becomes thinner.

6 Conclusion

We successfully fabricated stable and well-functioning TPB films on acrylic disks using a spin-coating method. We measured the thicknesses of the films as approximately 182 nm, and the surface was proven to be rather uniform based on an SEM analysis. We established an experimental setup to measure the optical properties of the TPB films. We checked the TPB reemission spectrum, which perfectly matches the result reported in a previous study [1]. The WLSE in our samples reached $25.1 \pm 4.4\%$ at the 95% C.L., which is similar to the TPB samples prepared using the vapor deposition method. The preliminary results show the feasibility of the spin-coating techniques, although for mass production, further research and development are required. The tuning parameters used in the spin-coating procedure will likely increase the WLSE and meet the requirements of different experiments. One of the shortcomings in the spin-coating method remains how to deal with large panels without a round shape. Current commercial instruments can no longer be applied. However, the relative velocity between the TPB liquid solution and the substrate meets the requirements of physics. For large-scale applications, we might have to spread the liquid solution onto the surface by adapting a well-designed jig and heater to fit the detector with a particular geometry. We will also have to improve the procedure for use in a clean room in the near future to avoid a radioactive background, which hinders the current technologies applied during the DM and the neutrino experiments. We expect this simple WLS coating technique to be optimized for future neutrino and dark matter detector constructions.

Acknowledgements This study was strongly supported by the Center for Fundamental Physics Laboratory in SYSU. We appreciate the help given by Prof. Han Shen and the technicians in his team. Many thanks to Prof. Yue Zheng and Prof. Wen-Peng Zhu for their help with the sample measurements using the SEM.

References

1. C. Benson, G. Orebi Gann, V. Gehman, Measurements of the intrinsic quantum efficiency and absorption length of tetraphenyl butadiene thin films in the vacuum ultraviolet regime. Eur. Phys. J. C **78**(78), 329 (2018). https://doi.org/10.1140/epjc/s10052-018-5807-z
2. M. Kuzniak, B. Broerman, T. Pollmann et al., Polyethylene naphthalate film as a wavelength shifter in liquid argon detectors. Eur. Phys. J. C **79**, 291 (2019). https://doi.org/10.1140/epjc/s10052-019-6810-8
3. D.M. Poehlmann, D. Barker, H. Chagani, et al., Characterization of gadolinium-loaded plastic scintillator for use as a neutron veto. arXiv:1812.11267 [physics.ins-det]
4. B. Fleming [MicroBooNE Collaboration], The MicroBooNE Technical Design Report https://doi.org/10.2172/1333130
5. B. Abi, R. Acciarri, M.A. Acero et al., [DUNE Collaboration], The DUNE far detector interim design report, Volume 2: single-phase module. arXiv:1807.10327 [physics.ins-det]
6. B. Broerman, M.G. Boulay, B. Cai et al., Application of the TPB wavelength shifter to the DEAP-3600 spherical acrylic vessel inner surface. JINST **12**(04), P04017 (2017). https://doi.org/10.1088/1748-0221/12/04/P04017
7. P.-A. Amaudruz, M. Baldwin, M. Batygov et al., [DEAP-3600 Collaboration], Design and construction of the DEAP-3600 dark matter detector. Astropart. Phys. **108**, 1 (2019). https://doi.org/10.1016/j.astropartphys.2018.09.006
8. C.E. Aalseth, F. Acerbi, P. Agnes et al., DarkSide-20k: a 20 tonne two-phase LAr TPC for direct dark matter detection at LNGS. Eur. Phys. J. Plus **133**, 131 (2018). https://doi.org/10.1140/epjp/i2018-11973-4
9. C. Amsler, A. Badertscher, V. Boccone et al., [ArDM Collaboration], First results on light readout from the 1-ton ArDM liquid argon detector for dark matter searches. JINST **5**, P11003 (2010). https://doi.org/10.1088/1748-0221/5/11/P11003
10. X. Dai, E. Rollin, A. Bellerive, C. Hargrove, D. Sinclair, C. Mifflin, F. Zhang, Wavelength shifters for water Cherenkov detectors. Nucl. Instrum. Meth. A **589**, 290 (2008). https://doi.org/10.1016/j.nima.2008.01.101
11. M. Sweany, A. Bernstein, S. Dazeley et al., Study of wavelength-shifting chemicals for use in large-scale water Cherenkov detectors. Nucl. Instrum. Meth. A **664**, 245 (2012). https://doi.org/10.1016/j.nima.2011.10.064
12. S. Joosten, E. Kaczanowicz, M. Ungaro et al., Enhanced UV light detection using a p-terphenyl wavelength shifter. Nucl. Instrum. Meth. A **870**, 110 (2017). https://doi.org/10.1016/j.nima.2017.06.050
13. M. Bonesini, T. Cervi, A. Falcone et al., An innovative technique for TPB deposition on convex window photomultiplier tubes. JINST **13**(12), P12020 (2018). https://doi.org/10.1088/1748-0221/13/12/P12020
14. B. Howard, S. Mufson, D. Whittington et al., A novel use of light guides and wavelength shifting plates for the detection of scintillation photons in large liquid argon detectors. Nucl. Instrum. Meth. A **907**, 9 (2018). https://doi.org/10.1016/j.nima.2018.06.050
15. R. Francini, R.M. Montereali, E. Nichelatti et al., VUV-Vis optical characterization of Tetraphenyl-butadiene films on glass and specular reflector substrates from room to liquid Argon temperature. JINST **8**(8), P09006 (2013). https://doi.org/10.1088/1748-0221/8/09/P09006
16. A. Bacchi, A. Brillante, D. Crocco et al., Exploration of the polymorph landscape for 1,1,4,4-tetraphenyl-1,3-butadiene. CrstEngComm **16**, 8205 (2014). https://doi.org/10.1039/C4CE01046A
17. A. Camposeo, M. Polo, P.D. Carro et al., Random lasing in an organic light-emitting crystal and its interplay with vertical cavity feedback. Laser Photoinics Rev. **8**, 785–291 (2014). https://doi.org/10.1002/lpor.201400031
18. A. Girlando, S. Ianelli, I. Bilotti et al., Spectroscopic and structural characterization of two polymorphs of 1,1,4,4-Tetraphenyl-1,3-butadiene. Cryst. Growth Des. **10**, 2752–2758 (2010). https://doi.org/10.1021/cg100253k
19. G. Hull, N.P. Zaitseva, N.J. Cherepy et al., New organic crystals for pulse shape discrimination. IEEEE Trans. Nucl. Sci. **56**, 899 (2009). https://doi.org/10.1109/TNS.2009.2015944
20. T. Pollmann, M. Boulay, M. Kuzniak, Scintillation of thin tetraphenyl butadiene films under alpha particle excitation. Nucl. Instrum. Meth. A **635**, 127 (2011). https://doi.org/10.1016/j.nima.2011.01.045

21. Z. Moss, L. Bugel, G. Collin et al., Improved TPB-coated light guides for liquid argon TPC light detection systems. JINST **10**, P08017 (2015). https://doi.org/10.1088/1748-0221/10/08/P08017
22. Y. Li, Q. Pan, J. Zhang et al., Preparation process of nanosized organic/inorganic thin films by sol-gel spin-coating method. J. Inorg. Mater. (2004). https://doi.org/10.3321/j.issn:1000-324X(2004)05-1065-08
23. D. Meyerhofer, Characteristics of resist films produced by spinning. J. Appl. Phys. **49**, 3993 (1978). https://doi.org/10.1063/1.325357
24. H. Yue, L. Pan, D. Xu, Evaporation and flow in the dye coating process. J. Tsinghua Univ. (Sci&Tech) **44**, 9 (2004). https://doi.org/10.16511/j.cnki.qhdxxb.2004.02.009. in Chinese
25. C.S. Chiu, C. Ignarra, L. Bugel et al., Environmental effects on TPB wavelength-shifting coatings. JINST **7**, P07007 (2012). https://doi.org/10.1088/1748-0221/7/07/P07007
26. B.J.P. Jones, J.K. VanGemert, J.M. Conrad et al., Photodegradation mechanisms of tetraphenyl butadiene coatings for liquid argon detectors. JINST **8**, P01013 (2013). https://doi.org/10.1088/1748-0221/8/01/P01013
27. A.G. Emslie, F.T. Bonner, L.G. Peck et al., Flow of a viscous liquid on a rotating disk. J. Appl. Phys. **29**, 858 (1958). https://doi.org/10.1063/1.1723300
28. https://oceanoptics.com/product/usb2000-custom/
29. https://www.kosakalab.co.jp/english/product/precision/minute/
30. http://www.cit17.com/cit17_Product_2056126605.html
31. http://setcas.com/?page_id=890
32. https://www.rigolna.com/products/digital-multimeters/dm3000/
33. Shen Zhen Long Xin Da Technology Electronic Co., Ltd, "Si Photodiode - LXD-66MQ Hand Book", 2019. (**in Chinese**)
34. P. Rau, Attenuation length measurements for DEAP-3600 light guide acrylic , DEAP-STR-2013-006 Rev 1
35. C. Joram, Transmission curves of plexiglass (PMMA) and optical grease, PH-EP-Tech-Note-2009-003 26/10/2009
36. NIST/SEMATECH e-Handbook of Statistical Methods, https://www.itl.nist.gov/div898/handbook/mpc/section5/mpc571.htm